Atmos. Chem. Phys., 18, 2821–2834, 2018
https://doi.org/10.5194/acp-18-2821-2018

Atmospheric Chemistry and Physics
Open Access
EGU

Dome effect of black carbon and its key influencing factors: a one-dimensional modelling study

Zilin Wang[1,2], **Xin Huang**[1,2], **and Aijun Ding**[1,2]

[1]Joint International Research Laboratory of Atmospheric and Earth System Sciences, School of Atmospheric Sciences, Nanjing University, Nanjing, 210023, China
[2]Jiangsu Provincial Collaborative Innovation Center of Climate Change, Nanjing, 210023, China

Correspondence: Xin Huang (xinhuang@nju.edu.cn)

Received: 16 October 2017 – Discussion started: 19 October 2017
Revised: 15 January 2018 – Accepted: 24 January 2018 – Published: 27 February 2018

Abstract. Black carbon (BC) has been identified to play a critical role in aerosol–planetary boundary layer (PBL) interaction and further deterioration of near-surface air pollution in megacities, which has been referred to as the "dome effect". However, the impacts of key factors that influence this effect, such as the vertical distribution and aging processes of BC, as well as the underlying land surface, have not been quantitatively explored yet. Here, based on available in situ measurements of meteorology and atmospheric aerosols together with the meteorology–chemistry online coupled model WRF-Chem, we conduct a set of parallel simulations to quantify the roles of these factors in influencing the BC dome effect and surface haze pollution. Furthermore, we discuss the main implications of the results to air pollution mitigation in China. We found that the impact of BC on the PBL is very sensitive to the altitude of aerosol layer. The upper-level BC, especially that near the capping inversion, is more essential in suppressing the PBL height and weakening the turbulent mixing. The dome effect of BC tends to be significantly intensified as BC mixed with scattering aerosols during winter haze events, resulting in a decrease in PBL height by more than 15 %. In addition, the dome effect is more substantial (up to 15 %) in rural areas than that in the urban areas with the same BC loading, indicating an unexpected regional impact of such an effect to air quality in countryside. This study indicates that China's regional air pollution would greatly benefit from BC emission reductions, especially those from elevated sources from chimneys and also domestic combustion in rural areas, through weakening the aerosol–boundary layer interactions that are triggered by BC.

1 Introduction

Air pollution, particularly haze pollution, has been one of the key environmental challenges for China, especially in the more developed regions like northern and eastern China (Wang et al., 2017). Haze pollution in these regions is generally characterized by extremely low visibility and dramatically rising surface aerosol concentration (Cai et al., 2017; Zhao et al., 2011). For example, in January 2013, a long-lasting episode of severe haze occurred in central and eastern China with a maximum $PM_{2.5}$ (particles with dynamic diameter less than 2.5 µm) mass concentration in Beijing reaching up to 680 µg m^{-3} (Wang et al., 2014a, c, d). In addition to deteriorating air quality in megacities like Beijing, large-scale regional haze pollution also covers rural and suburban areas (Xu et al., 2011; Chen and Wang, 2015). During serious haze pollution in that month, thick haze engulfed 1.4 million km^2 of land area, affecting up to 800 million people in 17 provinces. Such severe and aggravating regional haze pollution has triggered extensive public alarm due to $PM_{2.5}$-associated adverse health effects (e.g., cardiovascular and respiratory diseases) (Kim et al., 2015; Mauderly and Chow, 2008; Gao et al., 2015a; Pope et al., 2002). Consequently, air pollution mitigation has been one of the top priority for China's central and local governments. However, even though a series of control measures, such as the Action Plan on Prevention and Control of Air Pollution, have been carried out in order to reduce emissions and mitigate fine particle pollution (Zhang et al., 2016), the frequencies of severe pollution events have continued to increase in recent years and the intensity of pollution episodes has not shown a sig-

nificant decrease yet (Ding and Liu, 2013; Niu et al., 2010; Cai et al., 2017).

During hazy days, concentration of BC, one of the most important aerosol components from both environmental and climate perspectives, could exceed $20\,\mu g\,m^{-3}$ in China's megacities (Yang et al., 2007; Sun et al., 2014), higher than those in other regions across the world. Such a high level of BC concentration in China is primarily attributed to intensive residential combustions and a coal-dominant energy structure (Qin and Xie, 2011; Zhang et al., 2009b). With a high light-absorbing efficiency, BC can exert a substantial impact on climate change on a regional or even global scale (Bond et al., 2013; Menon et al., 2002; Ramanathan and Carmichael, 2008). At the same time, BC has been proven to be inextricably linked to short-term changes in public health such as cardiovascular mortality and cardiopulmonary hospital admissions (Eklund et al., 2014; Janssen et al., 2011). A recent study by Ding et al. (2016) has revealed the vital role of BC in enhancing near-surface haze pollution by the combined effects of heating by the light-absorbing BC aerosols in the upper PBL and the reduction of surface heat flux, which substantially suppresses the development of the PBL and consequently causes extreme haze pollution episodes in China's megacities. Such an effect has been referred to as the "dome effect" of BC (Ding et al., 2016). A similar effect has also been found for BC over the Indian Ocean (Wilcox et al., 2016) and dust aerosols in northern and eastern China (Liu et al., 2016; Yang et al., 2016).

In terms of the aerosol–PBL interaction induced by BC, the vertical distribution of the aerosol layer is expected to be an important influencing factor since the upper-level BC can alter the air temperature stratification much more efficiently (Ding et al., 2016). Located in one of the main monsoon regions, East China is subjected to large-scale monsoon circulations, where frequent cyclones, fronts and convections tend to lift near-surface air pollutants to the middle and even upper troposphere (Ding et al., 2009; Zhang et al., 2009a). In addition, elevated sources like power plant plumes and biomass burning smoke and subsequent long-range transport of air masses frequently lead to vertical heterogeneity of BC profile (Ding et al., 2013; Huang et al., 2016; Yang et al., 2015; Guinot et al., 2006; J. M. Chen et al., 2017). Thus, it is of great importance to understand the sensitivity of the dome effect to vertical distribution of BC in China. On the other hand, during haze events, it is highly possible that the coexistence of concentrated air pollutants and complex physicochemical interactions among them to lead to a dramatic increase in secondary aerosols (Huang et al., 2014a, b). Hence, freshly emitted BC has usually been observed to undergo notable aging and hygroscopic growth and become almost internally mixed with scattering secondary aerosols like sulfate during hazy days (Bond et al., 2013; Cui et al., 2016; Huang et al., 2013), thereby remarkably enhancing its light-absorbing properties (Peng et al., 2016; B. Chen et al., 2017; Cappa et al., 2012; Yang et al., 2012; Shen et al., 2017). Subsequently, the dome effect of BC might be significantly strengthened by mixing with scattering aerosols. However, such an influence of BC on the dome effect has not been quantitatively examined yet. As mentioned above, haze pollution has generally occurred on a regional scale in East and North China. Previous studies have highlighted the importance of aerosol–PBL interaction in cities (Petaja et al., 2016; Ding et al., 2016; Wang et al., 2014a; Gao et al., 2015b; Cai et al., 2017; Li et al., 2017b). It is noteworthy that more than half of the population lives in rural areas, with a majority in the plain areas in North and Central China, which has also been exposed to fine particulate pollution. The rural areas in East China are usually covered by cropland with different land-surface properties to urban areas. The difference of the dome effect over the two regions with distinct land cover categories remains to be further explored. In consequence, this study aims at identifying and quantitatively assessing the dependence of the dome effect on several key factors, including vertical distribution, aging of BC and the different underlying land surfaces (i.e., urban and rural areas).

Numerical simulation with meteorology–chemistry online coupled models has served as a practicable and effective way to characterize the aerosol radiative effect and its impact on PBL evolution (Grell et al., 2005; Baklanov et al., 2014; Yu et al., 2002). To disentangle the impacts of various factors on aerosol–PBL interaction, one-dimensional meteorology–chemistry online coupled model is applied in this study for the purpose of excluding influences from, for example, synoptic processes and regional transport. Additionally, one-dimensional modeling with high vertical resolution enables better representation of PBL evolution and also allows flexible initial and boundary conditions. Therefore, in the present work, a single-column version of WRF-Chem (Weather Research and Forecasting model coupled with Chemistry) driven by available observations is employed to investigate the aerosol–PBL interaction and its influencing parameters. The paper is organized as follows. Section 2 discusses major aspects of model simulations, including the WRF-Chem model and its configurations, parameterizations of aerosol properties, initial and boundary meteorological and chemical conditions, and the design of numerical experiments. The dome effect due to BC and its dependence on different conditions are presented and discussed in Sect. 3. Specifically, discussions in Sect. 3 include the effects of vertical distribution and aging process of BC, as well as different underlying land surfaces. Main results and the possible implications in future policy of air pollution mitigation are discussed in Sect. 4.

2 Data and method

2.1 Model configuration

The simulations were conducted with the WRF-Chem version 3.6.1 (Grell et al., 2005) single-column model (SCM). Except for advection, the physical and chemical processes are exactly the same as in the three-dimensional version, which is a fully coupled online meteorology–chemistry model including emission and deposition of pollutants, gaseous and aqueous chemical transformation, aerosol chemistry, and dynamics. The WRF-Chem SCM runs on a 3×3 grid with periodic lateral boundary conditions in both zonal and meridional directions. We used a spatial resolution of 4 km and a vertically stretched sigma coordinate with the model top set at a constant pressure, corresponding to about 6000 km. One hundred vertical levels were placed equidistantly with a height of 60 m from the ground surface to model top to better resolve the vertical structure of the atmosphere and ensure identical BC mass loadings.

The parameterization schemes were selected following the work by Ding et al. (2016), in which the model configuration showed good performance on boundary layer meteorology. The RRTMG short- and longwave radiation schemes (Iacono et al., 2008) were used to couple with aerosol scheme in order to reproduce aerosol–radiation interactions. The YSU nonlocal-K boundary layer scheme (Hong et al., 2006) and the Noah land surface scheme (Tewari et al., 2016) were applied for boundary layer evolution and land–atmosphere interactions, respectively. For representation of cloud and precipitation processes the Lin microphysics scheme (Lin, 1983) together with the Grell–Deveny cumulus parameterization (Grell and Devenyi, 2002) were employed. The CBMZ (Carbon Bond Mechanism version Z) photochemical mechanism combined with MOSAIC (Model for Simulating Aerosol Interactions and Chemistry) aerosol model (Fast et al., 2006; Zaveri and Peters, 1999) was applied to represent atmospheric chemistry. Aerosols were assumed to be spherical particles. The size distribution was divided into four discrete size bins defined by their lower and upper dry particle diameters (0.039–0.156, 0.156–0.625, 0.625–2.5 and 2.5–10.0 µm). Aerosol water content is calculated using the Zdanovskii–Stokes-Robinson method according to relative humidity (Zaveri et al., 2008). In each bin, aerosols are presumed to be spherical and internally mixed. The volume-averaged mixing rule is adopted to calculate the bulk refractive index by considering both aerosol water content and chemical compositions, including BC, sulfate, nitrate, and ammonium. Mie theory is then used to calculate the extinction coefficient, single-scattering albedo (SSA) along with asymmetry factor for each bin. Model domains and configuration selections are summarized in Table 1.

The WRF-Chem SCM was initialized with monthly averaged radio-sounding measurements at 12:00 UTC taken in Beijing (116.28° E, 39.93° N) to represent the typical atmospheric stratification in wintertime. Daily sounding data are archived at http://weather.uwyo.edu/upperair/sounding.html. The soil temperature profile was taken from the monthly averaged WRF regional simulation results for December 2013. The initial condition of atmospheric pollutants, which is mainly concerned with BC will be given in details in the following section. Vertical mixing of aerosol is switched off to ensure that the concentration and altitude of aerosol layer do not vary with PBL evolution. Each numerical experiment was conducted for a time period of 72 h with the first 48 h as model spin-up time.

Table 1. WRF-Chem SCM model settings and configuration options.

Domain setting	
Horizontal grid	3×3
Grid spacing	4 km
Vertical layers	100
Configuration options	
Longwave radiation	RRTMG
Shortwave radiation	RRTMG
Cumulus parameterization	Grell–Deveny
Land surface	unified Noah
Boundary layer	YSU
Microphysics	Lin (1983)
Gas-phase chemistry mechanism	CBMZ
Aerosol scheme	MOSAIC

2.2 Design and analysis of numerical experiments

We conducted a set of multidimensional experiments. Each individual experiment contains hundreds of simulations and can be divided into two groups. These two experiment groups shared exactly the same model settings and configurations except that one was with aerosol radiation interaction (ARI) and the other without (noARI). Each group consists of several parallel experiments with various initial conditions of airborne pollutants or surface parameters. To investigate the impact of heterogeneity in vertical distribution of BC on the dome effect, BC plumes with a width of 300 m were settled at different altitudes, ranging from the ground surface to about 2000 m. BC concentration was assumed to be 0–30 $\mu g\,m^{-3}$ according to existing field measurements across China (Zhang et al., 2013; Sun et al., 2004; Zhao et al., 2013a). BC concentrations in the plume were presumed to be a Gaussian distribution vertically, with a maximum value ranging from 0 to 30 $\mu g\,m^{-3}$ in the central axis, the altitude of which also ranges from 150 to 2250 m with an interval of 300 m.

Furthermore, to better understand the difference of the dome effect over different underlying ground surfaces (i.e., urban and rural areas) and its roles in regional air pollution,

Table 2. Distinctive differences of surface parameters between urban and rural land cover.

Properties	Urban and built-up land	Irrigated cropland and pasture
Albedo	0.15	0.2
Soil moisture	0.1	0.5
Emissivity	0.88	0.985
Roughness	80	2
Thermal inertia	3	4
Heat capacity	18.9×10^5	25.0×10^5

we conducted similar parallel numerical experiments over both urban and rural land surfaces. The distinct differences in important surface parameters between them are listed in Table 2. It is well known that BC emission is mainly related to fossil fuel combustion in China; hence, it is usually co-emitted with other gaseous pollutants like SO_2 and NO_x and then mixed with their oxidation products, i.e., sulfate and nitrate, during transportation and aging processes (Wang et al., 2014b; Huang et al., 2013; Cheng et al., 2006). To quantify the impact of mixing with these scattering aerosols, we also performed another two parallel simulations with different SNA (sulfate, nitrate and ammonium) aerosol concentration levels in the BC plume. The mass ratio of BC to SNA was derived from year-round measurement in Beijing (Zhang et al., 2013).

3 Results and discussion

3.1 One-dimensional modeling of the dome effect of BC

The dome effect of black carbon was first revealed by Ding et al. (2016) based on integrating online coupled regional simulation and corresponding observations during the winter haze event in December 2013, when severe $PM_{2.5}$ pollution covered East China with hourly concentrations up to $\sim 900\,\mu g\,m^{-3}$ and visibility less than 100 m (Zheng et al., 2015). In this study, it was proven that BC plays an important role in aggravating haze pollution via aerosol–PBL interaction. To clearly demonstrate BC-induced aerosol–PBL interaction, we selected one typical episode during 23–24 December 2013 in Beijing and initialized the WRF-Chem SCM with an averaged BC profile taken from three-dimensional simulation results for the same case by Ding et al. (2016). The regional WRF-Chem simulation of winter haze in December 2013 in Ding et al. (2016) had been verified to perform well in capturing the temporal variations of BC. The inputted BC vertical profile in Fig. 1 indicated that, during the abovementioned case, BC concentration reached up to approximately $30\,\mu g\,m^{-3}$ near the ground surface and decreased rapidly with altitude to a relatively constant value of

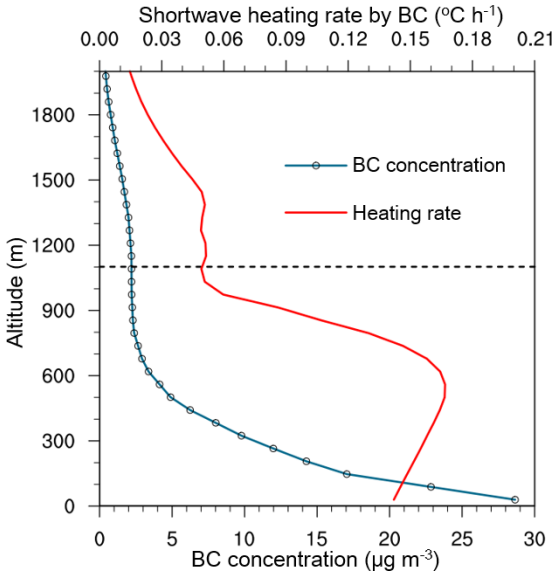

Figure 1. Vertical profiles of BC and shortwave heating rate included by unit BC mass in the afternoon (12:00–16:00 LT) during a heavily polluted episode on 23–24 December 2013 in Beijing. The black dashed line denotes the average PBL height during the same daytime period. The BC profile was extracted from regional WRF-Chem modeling by Ding et al. (2016).

less than $5\,\mu g\,m^{-3}$ above 800 m. However, although the BC profile featured its maximum concentration near the surface, the heating efficiency of BC due to shortwave radiation absorption peaked around 600–800 m, indicating that BC in the upper PBL is more efficient in terms of absorbing shortwave radiation and heating surrounding air masses. Such a heating profile is partly caused by the fact that incident solar radiation is attenuated by aerosols, trace gases and cloud when transferring within the atmosphere. Therefore, BC at higher altitudes tended to be subjected to higher incident radiation flux and absorb more solar energy. At the same time, lower air density caused the upper air to be more readily heated compared with that near the surface. Due to light absorption caused by BC together with additional extinction caused by scattering aerosols, solar radiation reaching the surface was diminished to a relatively large extent, resulting in less sensible heat flux and thus lower temperature in the near-surface atmosphere.

Overall, upper-level warming and surface cooling substantially modified the temperature stratification. As illustrated in Fig. 2, the afternoon upper-level heating and morning surface cooling could be clearly identified. The strongest upper-air warming had remained at over 1.0 °C between 1000 and 1200 m since midday (12:00 LT) because the incident shortwave radiation was most intense and the heating effect had already been accumulated before midday. The strongest cooling effect appeared in the morning (09:00–11:00 LT) and decreased very sharply after noon. The reason is that, with in-

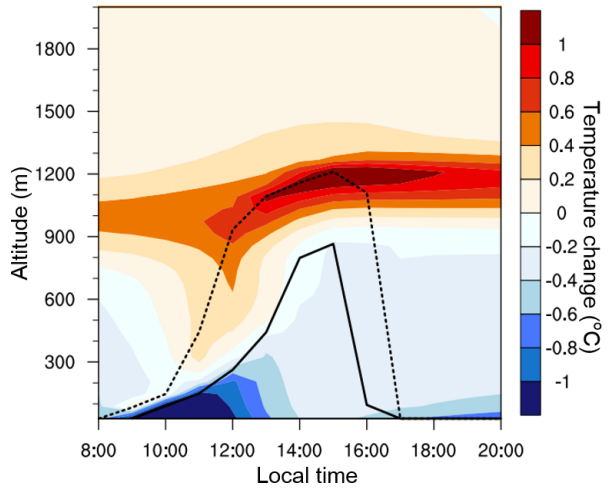

Figure 2. Diurnal variations of the air temperature change caused by aerosols during haze episodes in Beijing and of PBL height for simulation scenarios with (solid line) and without (dashed line) ARI.

creasingly intense turbulence during morning boundary evolution, part of the surface cooling was gradually compensated for by the entrainment of more warmed air into the turbulent PBL from above when the PBL was developed in the late morning. The warming and cooling of different atmospheric levels remarkably altered the stratification, thereby weakening convective motions. Stable stratification combined with decreased sensible heat flux at the ground surface greatly suppressed vertical turbulence in the boundary layer (Wilcox et al., 2016), contributing to a delay of PBL development and an earlier drop as well as a substantial decrease in PBL height, which hindered the air pollutants from being further dispersed vertically. These modifications in temperature stratification were relatively extensive in East China during winter according to the simulation conducted in Ding et al. (2016). For the whole month of December in 2013, the occurrence probability of enhanced atmospheric stability (PBL height decreasing over 10 %) due to the dome effect could reach up to 66, 73, 69 and 66 % in Zhengzhou, Shijiazhuang, Shanghai and Nanjing, respectively (Ding et al., 2016).

3.2 Impacts of altitude and concentration of BC aerosol layer

As previously mentioned, specific synoptic conditions, chimney plumes and regional transport of air pollution could result in non-uniformly distributed pollutant profiles (Xu et al., 2014; Guinot et al., 2006; Ding et al., 2009). Vertically inhomogeneous distribution of BC aerosol has been frequently observed by in situ aircraft and tethered balloon measurements (Zhao et al., 2015; Li et al., 2015). Given that BC was measured to rise around 800–1000 m during daytime in a haze episode (Li et al., 2015) and the upper-PBL BC has higher light-absorbing efficiency where solar heating usually maximizes, a BC plume with a maximum concentration of $10\,\mu g\,m^{-3}$ at the central axis is taken as a typical example to illustrate the perturbations on detailed physical processes related to PBL evolution due to a vertically non-uniform BC profile. As displayed in Fig. 3, with the existence of absorptive BC, incident solar radiation at the surface is diminished by about $5.9\,W\,m^{-2}$ at 12:00 LT, leading to a decline of 0.2 °C in surface temperature and a decline of $3.6\,W\,m^{-2}$ in surface sensible heat flux, which would otherwise heat the lower atmosphere, promote turbulent motions and enhance the PBL development. At the same time, absorbed radiation energy is converted to thermal energy and leads to substantial heating near the top of the PBL, as reflected by a rise in air temperature around 1.0 °C. Accordingly, modified temperature profile results in a more stable stratification with its exchange coefficient falling by 15 % (Fig. 3b), i.e., less turbulence mixing. Similarly, a substantial decrease in PBL height is attributed to less surface heat flux accompanied by stable stratification, which is showed in Fig. 3c.

To shed more light on the impacts of various BC vertical distributions on the dome effect, we conducted hundreds of parallel numerical experiments by changing the altitude and concentration magnitude of BC from the simulation shown in Fig. 3 to a larger extent in order to figure out how the PBL evolution responds to varying BC profiles and mass loading. Specifically, we manually increase BC concentrations from 0 to $30\,\mu g\,m^{-3}$ with an increment of $2\,\mu g\,m^{-3}$, all of which are placed at altitudes from 150 to 2250 m with an increment of 300 m. Thus, the multidimensional experiment consists of 105 parallel numerical simulations. All the individual simulations (marked by black dots in Fig. 4) and resultant perturbations on PBL height and the turbulence coefficient under different altitude and concentration loadings of BC are shown in Fig. 4. As several studies have pointed out, BC near the ground surface warms the Earth–atmosphere system and favors the development of the PBL by trapping more solar radiation that should be reflected by land and then promoting convective motions (Huang et al., 2015; Barbaro et al., 2014). The increased air temperature near the surface weakens the capping inversion, acting to cancel the effect of reduced buoyancy flux at the ground surface and raising the top of the PBL (Yu et al., 2002). However, this enhancement in PBL development is not that noticeable in magnitude while compared with PBL suppression due to BC at higher altitude. Consistent with several existing observational and numerical studies, absorbing smoke aloft is capable of remarkably changing the energy balance between the surface and the atmosphere in a way that stabilizes the boundary layer and suppresses convection (Koren et al., 2004; Ackerman et al., 2000). As demonstrated in Fig. 4, the PBL top could be decreased by about 15 % and the turbulent exchange coefficient dropped by over 20 % due to high-altitude BC plume. The substantial suppression effect induced by the BC plume maximizes around the top of the PBL and can be attributed

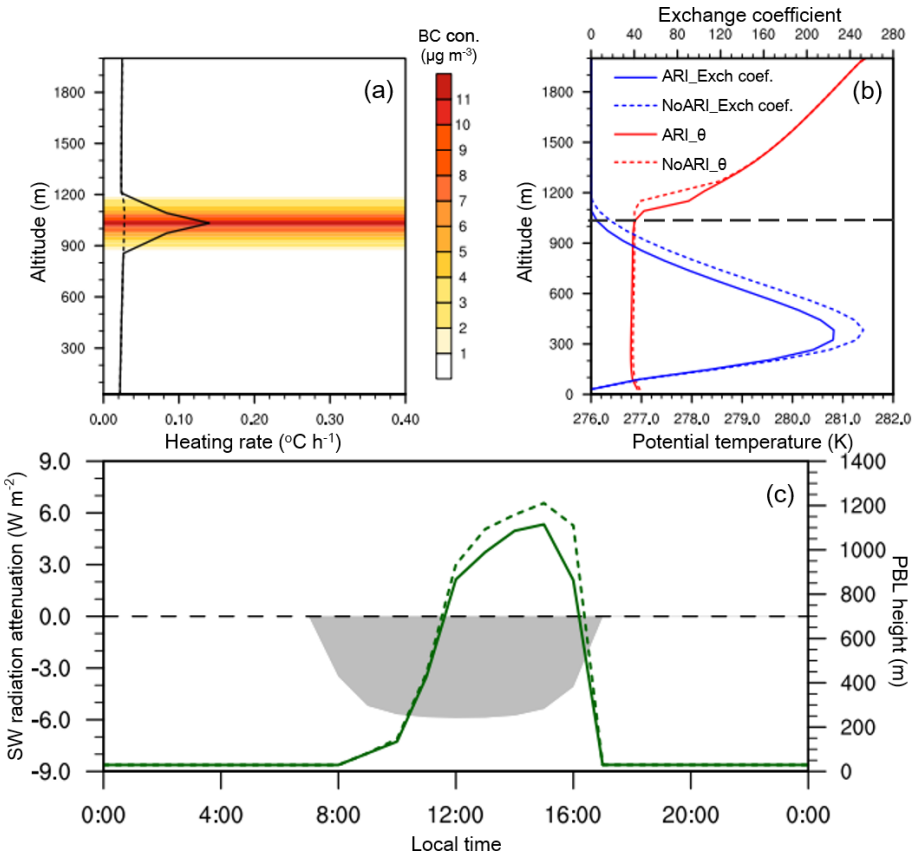

Figure 3. (a) Vertical distribution of BC aerosols (contour) and shortwave heating rate at 14:00 LT for runs with (solid line) and without (dashed line) ARI. **(b)** Vertical potential temperature profile (red) and exchange coefficient profile (blue) for runs with (solid line) and without (dashed line) ARI. The black dashed line represents the averaged PBL height during 12:00–16:00 LT. **(c)** Diurnal variations of PBL height for runs with (solid line) and without (dashed line) ARI and shortwave radiation attenuation at the surface induced by BC absorption.

to two main reasons. Firstly, incident solar radiation flux at the top of the PBL is usually most intense. After being absorbed by BC, it can effectively heat the surrounding air and change the strength of the capping inversion. Secondly, the turbulent exchange coefficient falls to a relatively small value when close to the top of the PBL (Fig. 3b), indicating that vertical turbulence exchange for heat at this height is rather weak. Therefore, the warming layer is prone to being kept at that level rather than diffusing vertically, further strengthening the capping inversion and consequently lowering the PBL height.

Another interesting fact is that, while BC layer is located above the original top of the PBL (i.e., above the 1300 m in Fig. 4), the boundary layer also becomes shallower but relatively less notable compared with upper-PBL BC layer (i.e., 600–1000 m). In this case, BC also blocks part of the incoming solar radiation and diminishes surface fluxes proportionally; nevertheless, it no longer alters the temperature stratification of the PBL below. It is well known that changes in the height of the PBL are determined by the surface buoyancy flux and the capping inversion, and both of them are affected by BC plumes (Ding et al., 2017, 2016). Since the impact of column loading of BC to surface buoyancy flux will not change substantially in the lower troposphere, here the different impact of BC on PBL height around the capping inversion (i.e., 600–1200 m) with the above altitudes indicates that the upper-air warming due to BC layer plays a more dominant role in depressing the PBL height and hence enhancing the near-surface air pollution.

3.3 Amplified dome effect by mixing with scattering aerosols

During wintertime heavily polluted episodes, when both primary and secondary pollutants increase dramatically, BC will be coated by scattering aerosols through condensation of low-volatility gases and coagulation with secondary aerosols and thus becomes hydrophilic and more internally mixed (Shiraiwa et al., 2007; Chen et al., 2016). Theoretically, its absorption properties can be significantly enhanced by internal mixing with other compounds because the coatings act as a lens and enlarge its mass absorption cross section effectively (Bond et al., 2013; B. Chen et al., 2017). Here, although organic matter also grows rapidly during hazy days,

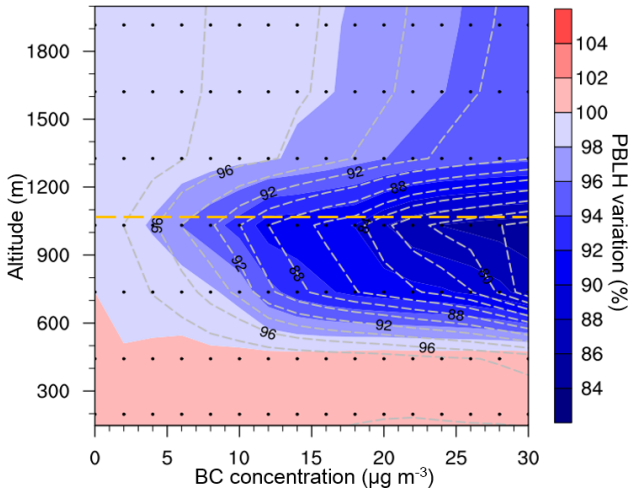

Figure 4. PBL height (contour map) and turbulence exchange coefficient (grey dashed isoline) variations in percentage as a function of the altitude and mass concentration of BC aerosol layers. Note: each dot on the figure represents an experiment with different BC input. The x axis gives concentrations in the center of the inputted BC plume, while the y axis gives the altitude of the residing plume. The yellow dashed line represents the original PBL height without any BC plume.

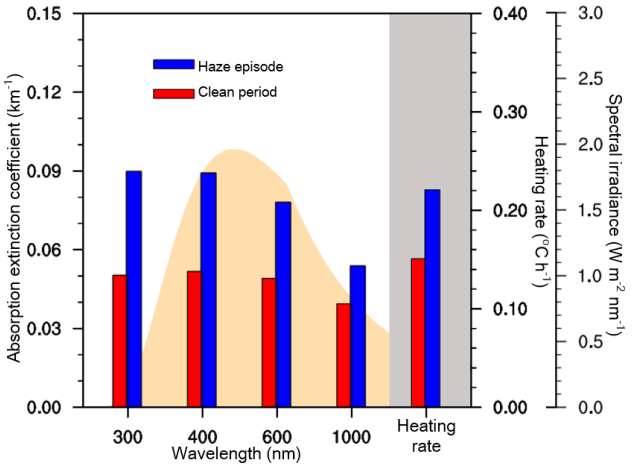

Figure 5. Aerosol absorption coefficient at different wavelengths (300, 400, 600, and 1000 nm) and shortwave heating rate at 12:00 LT for runs during a clean period and haze episode when the ratio of BC and SNA is 1 : 3 and 1 : 8, respectively. The yellow shaded area schematically shows solar spectral irradiance at sea level.

we do not include it in this work due to the uncertainties in its optical properties as well as less notable hygroscopicity. We analyzed this absorption amplification effect based on consistent in situ measurements during the development of severe haze pollution in Beijing in January 2013 (Sun et al., 2014). Compared with the clean period, the secondary aerosol increased significantly during haze episodes. Take sulfate aerosol for instance, its concentrations during hazy days were approximately 55 times higher than those under clean condition. Based on the ratio of BC to SNA during different periods and assuming BC concentration is 5 $\mu g\,m^{-3}$ (Zhang et al., 2013), absorption at the simulated wavelength (i.e., 300, 400, 600 and 1000 nm) was amplified by factors of 1.8, 1.7, 1.6 and 1.4, respectively (Fig. 5). These absorption coefficient amplification factors are comparable with in situ observations during clean period and haze event in the North China Plain (B. Chen et al., 2017). To investigate the relative importance of amplified absorption for each band, the solar spectral irradiance at sea level is also given for reference. The absorptive magnification for radiation at the wavelength of 400–600 nm tends to have a dominant effect since the solar irradiance peaks in this band. Accordingly, shortwave heating rate also increased from about 0.15 to over 0.22 $K\,h^{-1}$, which considerably accelerates the warming effect induced by BC (Fig. 5).

In addition to directly increasing the absorption cross section, SNA could undergo deliquescence and lead to an increase in aerosol diameter to a large extent, especially under humid conditions, indirectly enhancing the light-absorbing capacity (Tsai and Kuo, 2005; Zheng et al., 2015; Liu et al., 2011). To comprehensively understand this enhancement effect induced by SNA, we conducted tens of sensitivity experiments under different levels of SNA concentration and relative humidity (RH). As presented in Fig. 6, aerosol absorption extinction coefficient increases with SNA concentration. This dependence on SNA is much notable under lower RH (50 %) before aerosol starts to deliquesce. By contrast, when the air becomes more humid, aerosol water uptake becomes increasingly more important. According to year-round observational data (Zhang et al., 2012), SNA concentrations and humidity condition vary a lot across China. For typical cities in China, the annual-averaged SNA level ranges from 40–60 $\mu g\,m^{-3}$ in Nanjing (118.95° E, 32.12° N) and Shanghai (121.45° E, 31.22° N) to almost 140 $\mu g\,m^{-3}$ in Beijing (116.30° E, 39.99° N), but the annual mean BC concentrations are approximately 5 $\mu g\,m^{-3}$ (Ye et al., 2003; Zhang et al., 2013). In Nanjing, with a lower SNA level but higher RH, SNA-induced hygroscopic growth may play the dominant role in the enhancement of aerosol light-absorbing efficiency. Instead, relatively higher SNA concentration in Beijing makes the main contribution according to Fig. 6. Specifically, the absorption could be elevated by 63 % when RH rises from 50 to 90 % in Nanjing, while for Beijing the corresponding enhancement is only 18 %. Such disparities indicate that aerosol absorption and further impact on boundary layer evolution have a closer link to humidity and will be more important in coastal region at lower latitudes in China.

Enhanced light absorption and heating efficiency by mixing with SNA certainly perturb aerosol–PBL interactions (Fig. 7). Overall, the PBL responses tend to be magnified in terms of both increased PBL top by near-surface BC and

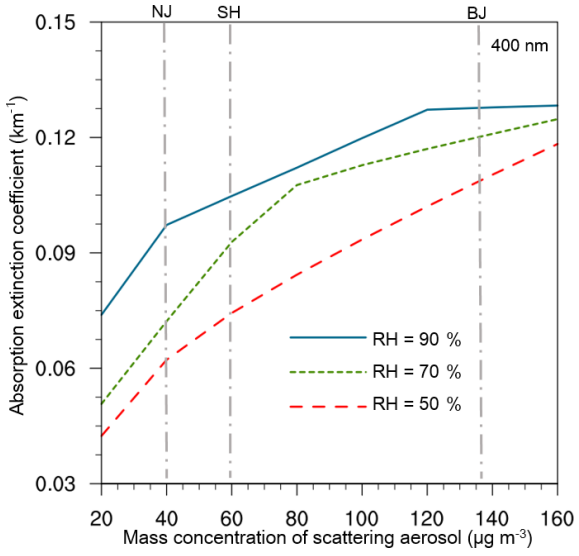

Figure 6. Variation of absorption extinction coefficient at 400 nm as a function of different mass concentrations of scattering aerosols mixing with BC. The BC concentration is fixed at $5\,\mu g\,m^{-3}$ under various moisture conditions of relative humidity, i.e., 50, 70 and 90 %. Three main cities (BJ, SH and NJ) are marked in the figure with their annual mean $PM_{2.5}$ concentrations.

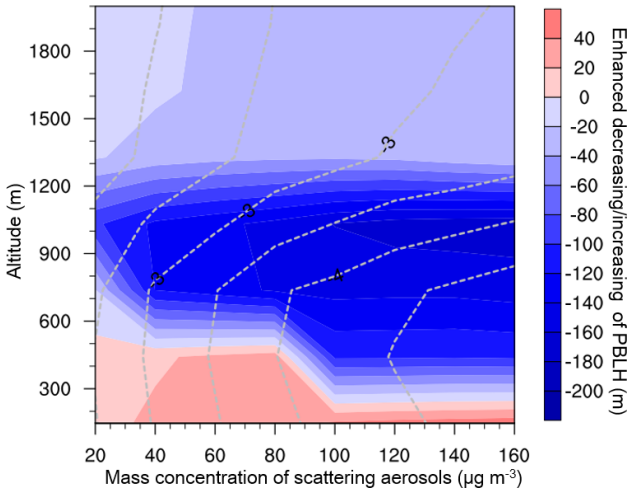

Figure 7. Enhanced decreasing/increasing of PBL height (contour map) and enhanced reduction of sensible heat flux at surface (dashed isoline) caused by amplified absorption of BC internally mixed with scattering aerosols. BC concentration is fixed at $5\,\mu g\,m^{-3}$, and the ratio of scattering aerosol components is SO_4^{2-} : NO_3^- : $NH_4^+ = 3:2:1$, which is based on year-round observations in Beijing (Zhang et al., 2012). The x and y axes are the same as Fig. 4.

suppressed convections by upper-level BC. For typical wintertime meteorological conditions in Beijing, aging processes could lead to a decline of $5\,W\,m^{-2}$ in surface heat flux and an additional 15 % decrease in the PBL top at a maximum when compared with those caused by freshly emitted BC. What is more, when BC concentration is fixed at $5\,\mu g\,m^{-3}$ and SNA concentration exceeds $80\,\mu g\,m^{-3}$, this absorption enhancement leads to the phenomenon that even BC at lower altitudes may increase the stratification and exert a negative effect on PBL development, as shown in Fig. 7. However, this abrupt change is not observed in simulations with only SNA aerosols included. In other words, there probably exists a critical point of the BC/SNA ratio for its associated dome effect, from which the impact of lower-level BC on PBL suppression would be oppositely attributed to a large decrease in surface sensible heat flux.

3.4 A comparison of the dome effect over urban and rural areas

In the past, BC-induced aerosol–PBL interaction has mostly been investigated for cities. However, urban areas only take up approximately 5 % of the area in China, while cropland is the dominant surface type and also features dense population and high $PM_{2.5}$ exposure (Liu, 2005; Xu et al., 2011). Frequent regional-scale haze pollution and cropland-dominant land cover in China make it necessary to understand this interaction over rural areas (Yang et al., 2015; Zhao et al., 2013b). The differences in surface parameters between cities and rural area are listed in Table 2. Comparatively, rural surfaces, including cropland and pasture, are characterized by larger surface albedo, higher soil moisture and greater heat capacity.

The radiation energy balance without any influence from aerosol already shows great disparities for the two kinds of land surface. Under the same level of incident solar radiation intensity, net shortwave radiation at the ground surface is mainly determined by land surface albedo. In comparison with urban areas, less net downward solar radiation on rural surfaces is ascribed to larger albedo reflecting more solar radiation, accompanied by higher upwards shortwave radiation flux at the top of the atmosphere, as shown in Fig. 8. Correspondingly, the surface temperature in rural areas at noon is almost 1.5 °C colder than that in urban areas, indicating a strong urban heat island effect (Oke, 1982). As for the atmospheric heating, there is little difference over both surface types when excluding the radiative perturbation of aerosols. The resultant height of the PBL is expected to be 250 m lower in rural areas.

If taking the aerosol radiative effect into account when BC is $10\,\mu g\,m^{-3}$ around an altitude of 1000 m, over both urban and rural areas, net downward shortwave radiation flux, surface temperature and upwelling shortwave radiation show a notable decrease. At the same time, atmospheric heating rate in the upper air increases in response. The most distinctive difference between these two kinds of land surface is that upwelling shortwave radiation flux at the top of the atmosphere over rural surfaces shows a reduction twice high as over urban surfaces, indicating that a larger portion of so-

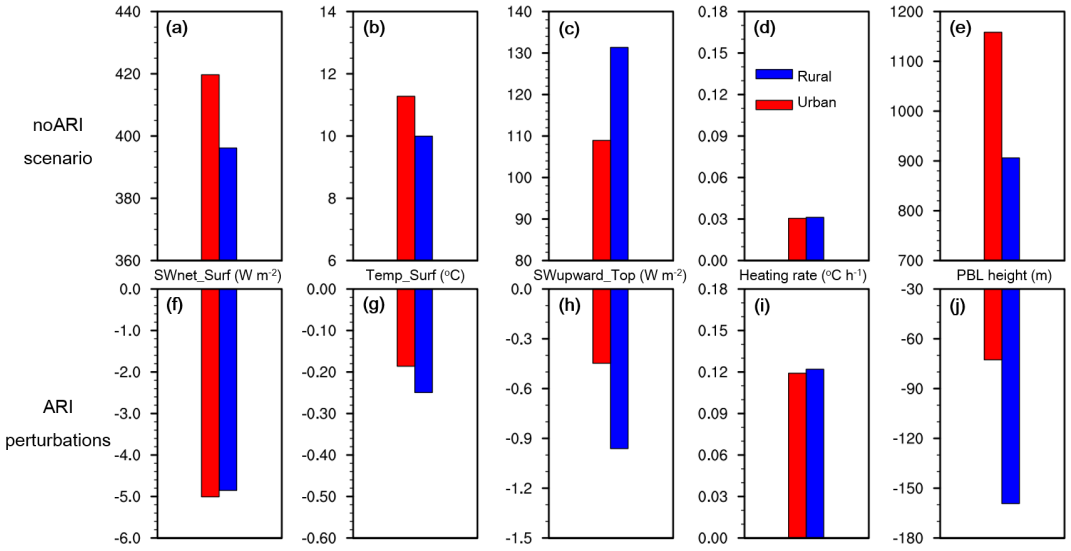

Figure 8. Net downward shortwave radiation at surface (SWnet_Surf), surface temperature (Temp_Surf), upwelling shortwave radiation at model top (SWupward_Top) and shortwave heating rate, PBL height for urban and rural underlying surfaces without aerosol effect **(a–e)**, and their corresponding perturbations due to aerosol–boundary layer interaction **(f–j)**.

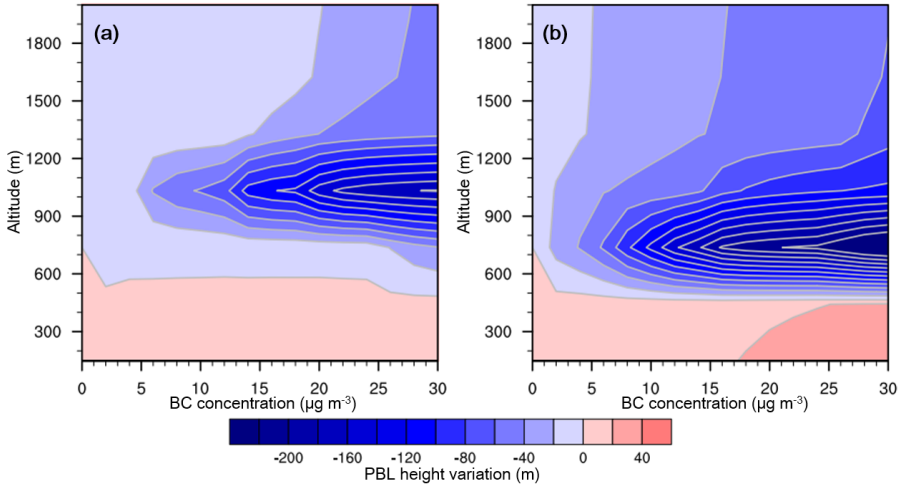

Figure 9. Different PBL height variations due to specific BC distribution over **(a)** urban surface and **(b)** rural land surface. The *x* and *y* axes are the same as Fig. 4.

lar energy is blocked in the atmosphere, which corresponds to a much stronger atmospheric heating rate due to radiation absorption. At the same time, it suggests a slightly larger decrease in surface temperature over rural surfaces, followed by a lower sensible heat transfer into the atmosphere. The greater surface cooling together with more intense upper warming jointly enhances stable stratification. Therefore, the decrease in the PBL top in rural areas is double that in cities, as shown in Fig. 8.

A comprehensive analysis of responses of the PBL to various magnitudes and altitudes of BC aerosol over urban and rural land surfaces is illustrated in Fig. 9. As mentioned before, since the PBL is less well developed in rural area, the altitude of the BC plume with maximum suppression effect on the PBL was slightly lower than that over cities. Additionally, BC-induced heating is more intensive over rural surfaces due to the fact that larger albedo results in more shortwave radiation reflected by the ground surface, part of which is absorbed by BC aerosol when transferring upwards. Consequently, the promotion and suppression effect on the PBL attributed to BC aerosol over rural surfaces is about 15 % larger than that over urban surfaces. That is, BC would exert a more intense dome effect over rural surfaces. It should be noted that residential combustion of raw coal and biofuel

in a small domestic stove in rural area is responsible for the majority of BC emission in China (Zhi et al., 2008; Li et al., 2017a). A more stable PBL and more significant dome effect over rural surfaces would further favor the formation and accumulation of regional air pollution.

4 Summary and implications

The dome effect of BC plays a crucial role in air pollution deterioration, which is expected to be highly dependent on many factors like vertical distribution, mass loading, and aging processes of BC as well as the underlying land surface. By integrating available in situ observations of meteorology and atmospheric aerosols together with simulations using meteorology–chemistry online coupled model WRF-Chem SCM, we conduct a set of multidimensional experiments, each of which contains hundreds of parallel simulations, to quantify the impacts of these factors in enhancing the surface haze pollution. We found that the dome effect of BC is extremely sensitive to the altitude of aerosol layer. In more detail, near-surface BC tends to promote the PBL development, while BC aloft is more essential in PBL suppression, especially near the capping inversion. At the same time, this work indicates that the dome effect of BC can be significantly intensified when BC gets internally mixed with scattering aerosol during winter haze events, which could further decrease PBL height by up to 15 %. In terms of different underlying surface, the dome effect is more substantial in rural areas. Under the same conditions of BC, the PBL top decrease in rural areas could be 15 % greater than the corresponding value in urban areas.

Haze pollution in China is becoming increasingly frequent and thus has received extensive attention from the public and government. In spite of a series of emission control measures, the air quality has yet to be improved substantially, especially for the extreme haze events in winter. Our study highlights the importance of BC in worsening air pollution and further provides clues for both long-term policy making on air quality improvement and short-term pollution emergency plan. Our study has shown that the long-range transport of absorption aerosols like BC could cause a larger impact on regional air quality. In fact, the elevated emission sources, i.e., point sources with chimneys like coal-fired power plants that are typically higher than 200 m, could be easily transported and deteriorate dispersion conditions by suppressing the PBL on larger scales. Therefore, an efficient way to mitigate near-surface air pollution is to preferentially reduce BC emission from these sources before and during regional severe haze pollution. In the longer run, clean energy substitution and extension of BC emission reduction technologies should be encouraged. In addition, it is noteworthy that residential combustion is responsible for the majority of pollution sources in the countryside/rural areas and is the most important contributor to BC emissions in China, which could be lifted to the upper PBL through convective motions. Considering the significant dome effect of BC over rural surfaces, the residential combustion sources would further favor the formation and deterioration of regional air pollution. As a result, it can be implied that abatement technology for domestic stoves in rural areas could be another cost-effective way to reduce regional air pollution. Of course, as one of the key short-lived climate forcers, BC has been found to be one of the most important components contributing to global warming. These efforts devoted to reducing BC emission in both urban and rural areas in China definitely result in a substantial reduction in the national carbon emission and co-benefit the mitigation of global warming.

In addition, our study here highlights the significance of investigating the vertical structure of atmospheric processes in detail in the lower atmosphere, which is very important for improving the understanding of the interaction of atmospheric physics and chemistry. However, in China, most of the existing and current efforts of field measurements, including both routinely operated monitoring networks and research based field measurement stations, have been mainly focused on the ground surface. There is very limited information on the vertical profiles of atmospheric aerosols and physical parameters related to key processes in the PBL. For numerical models, there is also a lack of vertical datasets for model evaluation and parameterization improvement. To gain a more comprehensive understanding of the causes and evolution of air pollution, more vertical measurements – including in situ measurements based on aircraft and tagged balloon platforms and remote sensing measurements using ground-based instruments and satellites – are urgently needed in the near future.

Data availability. Radiosonde observations used in this work can be acquired from http://weather.uwyo.edu/upperair/sounding.html. Model outputs are stored in the server of School of Atmospheric Sciences at Nanjing University and are available upon request from the corresponding author.

Acknowledgements. This work was supported by the National Natural Science Foundation of China (D0512/91544231, D0510/41725020, D0512/41422504, and D0510/41505109). Part of this work was supported by the Ministry of Science and Technology of the People's Republic of China (2016YFC0200500), the Public Welfare Projects for Environmental Protection (201509004) and Jiangsu Provincial 2011 program (Collaborative Innovation Center of Climate Change).

Edited by: Qiang Zhang
Reviewed by: two anonymous referees

References

Ackerman, A. S., Toon, O. B., Stevens, D. E., Heymsfield, A. J., Ramanathan, V., and Welton, E. J.: Reduction of tropical cloudiness by soot, Science, 288, 1042–1047, https://doi.org/10.1126/science.288.5468.1042, 2000.

Baklanov, A., Schlünzen, K., Suppan, P., Baldasano, J., Brunner, D., Aksoyoglu, S., Carmichael, G., Douros, J., Flemming, J., Forkel, R., Galmarini, S., Gauss, M., Grell, G., Hirtl, M., Joffre, S., Jorba, O., Kaas, E., Kaasik, M., Kallos, G., Kong, X., Korsholm, U., Kurganskiy, A., Kushta, J., Lohmann, U., Mahura, A., Manders-Groot, A., Maurizi, A., Moussiopoulos, N., Rao, S. T., Savage, N., Seigneur, C., Sokhi, R. S., Solazzo, E., Solomos, S., Sørensen, B., Tsegas, G., Vignati, E., Vogel, B., and Zhang, Y.: Online coupled regional meteorology chemistry models in Europe: current status and prospects, Atmos. Chem. Phys., 14, 317–398, https://doi.org/10.5194/acp-14-317-2014, 2014.

Barbaro, E., de Arellano, J. V. G., Ouwersloot, H. G., Schroter, J. S., Donovan, D. P., and Krol, M. C.: Aerosols in the convective boundary layer: shortwave radiation effects on the coupled land–atmosphere system, J. Geophys. Res.-Atmos., 119, 5845–5863, https://doi.org/10.1002/2013JD021237, 2014.

Bond, T. C., Doherty, S. J., Fahey, D. W., Forster, P. M., Berntsen, T., DeAngelo, B. J., Flanner, M. G., Ghan, S., Kärcher, B., Koch, D., Kinne, S., Kondo, Y., Quinn, P. K., Sarofim, M. C., Schultz, M. G., Schulz, M., Venkataraman, C., Zhang, H., Zhang, S., Bellouin, N., Guttikunda, S. K., Hopke, P. K., Jacobson, M. Z., Kaiser, J. W., Klimont, Z., Lohmann, U., Schwarz, J. P., Shindell, D., Storelvmo, T., Warren, S. G., and Zender, C. S.: Bounding the role of black carbon in the climate system: a scientific assessment, J. Geophys. Res.-Atmos., 118, 5380–5552, https://doi.org/10.1002/jgrd.50171, 2013.

Cai, W. J., Li, K., Liao, H., Wang, H. J., and Wu, L. X.: Weather conditions conducive to Beijing severe haze more frequent under climate change, Nat. Clim. Change, 7, 257, https://doi.org/10.1038/Nclimate3249, 2017.

Cappa, C. D., Onasch, T. B., Massoli, P., Worsnop, D. R., Bates, T. S., Cross, E. S., Davidovits, P., Hakala, J., Hayden, K. L., Jobson, B. T., Kolesar, K. R., Lack, D. A., Lerner, B. M., Li, S.-M., Mellon, D., Nuaaman, I., Olfert, J. S., Petäjä, T., Quinn, P. K., Song, C., Subramanian, R., Williams, E. J., and Zaveri, R. A.: Radiative absorption enhancements due to the mixing state of atmospheric black carbon, Science, 337, 1078–1081, https://doi.org/10.1126/science.1223447, 2012.

Chen, H. and Wang, H.: Haze days in North China and the associated atmospheric circulations based on daily visibility data from 1960 to 2012, J. Geophys. Res.-Atmos., 120, 5895–5909, https://doi.org/10.1002/2015jd023225, 2015.

Chen, Y., Cao, J., Huang, R., Yang, F., Wang, Q., and Wang, Y.: Characterization, mixing state, and evolution of urban single particles in Xi'an (China) during wintertime haze days, Sci. Total Environ., 573, 937–945, https://doi.org/10.1016/j.scitotenv.2016.08.151, 2016.

Chen, B., Bai, Z., Cui, X., Chen, J., Andersson, A., and Gustafsson, O.: Light absorption enhancement of black carbon from urban haze in Northern China winter, Environ. Pollut., 221, 418–426, https://doi.org/10.1016/j.envpol.2016.12.004, 2017.

Chen, J. M., Li, C. L., Ristovski, Z., Milic, A., Gu, Y. T., Islam, M. S., Wang, S. X., Hao, J. M., Zhang, H. F., He, C. R., Guo, H., Fu, H. B., Miljevic, B., Morawska, L., Thai, P., Fat, L. A. M. Y., Pereira, G., Ding, A. J., Huang, X., and Dumka, U. C.: A review of biomass burning: emissions and impacts on air quality, health and climate in China, Sci. Total Environ., 579, 1000–1034, 2017.

Cheng, Y. F., Eichler, H., Wiedensohler, A., Heintzenberg, J., Zhang, Y. H., Hu, M., Herrmann, H., Zeng, L. M., Liu, S., Gnauk, T., Bruggemann, E., and He, L. Y.: Mixing state of elemental carbon and non-light-absorbing aerosol components derived from in situ particle optical properties at Xinken in Pearl River Delta of China, J. Geophys. Res.-Atmos., 111, D20204, https://doi.org/10.1029/2005JD006929, 2006.

Cui, X., Wang, X., Yang, L., Chen, B., Chen, J., Andersson, A., and Gustafsson, O.: Radiative absorption enhancement from coatings on black carbon aerosols, Sci. Total Environ., 551, 51–56, https://doi.org/10.1016/j.scitotenv.2016.02.026, 2016.

Ding, Y. and Liu, Y.: Analysis of long-term variations of fog and haze in China in recent 50 years and their relations with atmospheric humidity, Sci. China Earth Sci., 57, 36–46, https://doi.org/10.1007/s11430-013-4792-1, 2013.

Ding, A. J., Wang, T., Xue, L. K., Gao, J., Stohl, A., Lei, H. C., Jin, D. Z., Ren, Y., Wang, X. Z., Wei, X. L., Qi, Y. B., Liu, J., and Zhang, X. Q.: Transport of north China air pollution by midlatitude cyclones: case study of aircraft measurements in summer 2007, J. Geophys. Res.-Atmos., 114, D08304, https://doi.org/10.1029/2008jd011023, 2009.

Ding, A. J., Fu, C. B., Yang, X. Q., Sun, J. N., Petäjä, T., Kerminen, V.-M., Wang, T., Xie, Y., Herrmann, E., Zheng, L. F., Nie, W., Liu, Q., Wei, X. L., and Kulmala, M.: Intense atmospheric pollution modifies weather: a case of mixed biomass burning with fossil fuel combustion pollution in eastern China, Atmos. Chem. Phys., 13, 10545–10554, https://doi.org/10.5194/acp-13-10545-2013, 2013.

Ding, A. J., Huang, X., Nie, W., Sun, J. N., Kerminen, V. M., Petäjä, T., Su, H., Cheng, Y. F., Yang, X. Q., Wang, M. H., Chi, X. G., Wang, J. P., Virkkula, A., Guo, W. D., Yuan, J., Wang, S. Y., Zhang, R. J., Wu, Y. F., Song, Y., Zhu, T., Zilitinkevich, S., Kulmala, M., and Fu, C. B.: Enhanced haze pollution by black carbon in megacities in China, Geophys. Res. Lett., 43, 2873–2879, https://doi.org/10.1002/2016gl067745, 2016.

Ding, A., Huang, X., and Fu, C.: Air pollution and weather interaction in east Asia, Oxford Research Encyclopedias-Environmental Science, 1, 1–26, https://doi.org/10.1093/acrefore/9780199389414.013.536, 2017.

Eklund, A. G., Chow, J. C., Greenbaum, D. S., Hidy, G. M., Kleinman, M. T., Watson, J. G., and Wyzga, R. E.: Public health and components of particulate matter: the changing assessment of black carbon, J. Air Waste Manage., 64, 1221–1231, https://doi.org/10.1080/10962247.2014.960218, 2014.

Fast, J. D., Gustafson Jr., W. I., Easter, R. C., Zaveri, R. A., Barnard, J. C., Chapman, E. G., Grell, G. A., and Peckham, S. E.: Evolution of ozone, particulates, and aerosol direct radiative forcing in the vicinity of Houston using a fully coupled meteorology-chemistry-aerosol model, J. Geophys. Res.-Atmos., 111, 5173–5182, 2006.

Gao, M., Guttikunda, S. K., Carmichael, G. R., Wang, Y. S., Liu, Z. R., Stanier, C. O., Saide, P. E., and Yu, M.: Health impacts and economic losses assessment of the 2013 severe haze event in Beijing area, Sci. Total Environ., 511, 553–561, 2015a.

Gao, Y., Zhang, M., Liu, Z., Wang, L., Wang, P., Xia, X., Tao, M., and Zhu, L.: Modeling the feedback between aerosol and meteorological variables in the atmospheric boundary layer during a severe fog–haze event over the North China Plain, Atmos. Chem. Phys., 15, 4279–4295, https://doi.org/10.5194/acp-15-4279-2015, 2015b.

Grell, G. and Devenyi, D.: A generalized approach to parameterizing convection combining ensemble and data assimilation, Geophys. Res. Lett., 29, 1693, https://doi.org/10.1029/2002GL015311, 2002.

Grell, G. A., Peckham, S. E., Schmitz, R., McKeen, S. A., Frost, G., Skamarock, W. C., and Eder, B.: Fully coupled "online" chemistry within the WRF model, Atmos. Environ., 39, 6957–6975, https://doi.org/10.1016/j.atmosenv.2005.04.027, 2005.

Guinot, B., Roger, J.-C., Cachier, H., Pucai, W., Jianhui, B., and Tong, Y.: Impact of vertical atmospheric structure on Beijing aerosol distribution, Atmos. Environ., 40, 5167–5180, https://doi.org/10.1016/j.atmosenv.2006.03.051, 2006.

Hong, S.-Y., Noh, Y., and Dudhia, J.: A new vertical diffusion package with an explicit treatment of entrainment processes, Mon. Weather Rev., 134, 2318–2341, https://doi.org/10.1175/MWR3199.1, 2006.

Huang, X.-F., Xue, L., Tian, X.-D., Shao, W.-W., Sun, T.-L., Gong, Z.-H., Ju, W.-W., Jiang, B., Hu, M., and He, L.-Y.: Highly time-resolved carbonaceous aerosol characterization in Yangtze River Delta of China: composition, mixing state and secondary formation, Atmos. Environ., 64, 200–207, https://doi.org/10.1016/j.atmosenv.2012.09.059, 2013.

Huang, R. J., Zhang, Y. L., Bozzetti, C., Ho, K. F., Cao, J. J., Han, Y. M., Daellenbach, K. R., Slowik, J. G., Platt, S. M., Canonaco, F., Zotter, P., Wolf, R., Pieber, S. M., Bruns, E. A., Crippa, M., Ciarelli, G., Piazzalunga, A., Schwikowski, M., Abbaszade, G., Schnelle-Kreis, J., Zimmermann, R., An, Z. S., Szidat, S., Baltensperger, U., El Haddad, I., and Prevot, A. S. H.: High secondary aerosol contribution to particulate pollution during haze events in China, Nature, 514, 218–222, https://doi.org/10.1038/nature13774, 2014a.

Huang, X., Song, Y., Zhao, C., Li, M. M., Zhu, T., Zhang, Q., and Zhang, X. Y.: Pathways of sulfate enhancement by natural and anthropogenic mineral aerosols in China, J. Geophys. Res.-Atmos., 119, 14165–14179, https://doi.org/10.1002/2014JD022301, 2014b.

Huang, X., Song, Y., Zhao, C., Cai, X., Zhang, H., and Zhu, T.: Direct radiative effect by multicomponent aerosol over China, J. Climate, 28, 3472–3495, https://doi.org/10.1175/jcli-d-14-00365.1, 2015.

Huang, X., Ding, A., Liu, L., Liu, Q., Ding, K., Niu, X., Nie, W., Xu, Z., Chi, X., Wang, M., Sun, J., Guo, W., and Fu, C.: Effects of aerosol–radiation interaction on precipitation during biomass-burning season in East China, Atmos. Chem. Phys., 16, 10063–10082, https://doi.org/10.5194/acp-16-10063-2016, 2016.

Iacono, M. J., Delamere, J. S., Mlawer, E. J., Shephard, M., Clough, S., and Collins, W.: Radiative forcing by long-lived greenhouse gases: calculations with the AER radiative transfer models, J. Geophys. Res.-Atmos., 113, D13103, https://doi.org/10.1029/2008JD009944, 2008.

Janssen, N. A. H., Hoek, G., Simic-Lawson, M., Fischer, P., van Bree, L., ten Brink, H., Keuken, M., Atkinson, R. W., Anderson, H. R., Brunekreef, B., and Cassee, F. R.: Black carbon as an additional indicator of the adverse health effects of airborne particles compared with PM_{10} and $PM_{2.5}$, Environ. Health Persp., 119, 1691–1699, https://doi.org/10.1289/ehp.1003369, 2011.

Kim, K.-H., Kabir, E., and Kabir, S.: A review on the human health impact of airborne particulate matter, Environ. Int., 74, 136–143, https://doi.org/10.1016/j.envint.2014.10.005, 2015.

Koren, I., Kaufman, Y. J., Remer, L. A., and Martins, J. V.: Measurement of the effect of Amazon smoke on inhibition of cloud formation, Science, 303, 1342–1345, https://doi.org/10.1126/science.1089424, 2004.

Li, J., Fu, Q. Y., Huo, J. T., Wang, D. F., Yang, W., Bian, Q. G., Duan, Y. S., Zhang, Y. H., Pan, J., Lin, Y. F., Huang, K., Bai, Z. P., Wang, S. H., Fu, J. S., and Louie, P. K. K.: Tethered balloon-based black carbon profiles within the lower troposphere of Shanghai in the 2013 East China smog, Atmos. Environ., 123, 327–338, https://doi.org/10.1016/j.atmosenv.2015.08.096, 2015.

Li, M., Zhang, Q., Kurokawa, J.-I., Woo, J.-H., He, K., Lu, Z., Ohara, T., Song, Y., Streets, D. G., Carmichael, G. R., Cheng, Y., Hong, C., Huo, H., Jiang, X., Kang, S., Liu, F., Su, H., and Zheng, B.: MIX: a mosaic Asian anthropogenic emission inventory under the international collaboration framework of the MICS-Asia and HTAP, Atmos. Chem. Phys., 17, 935–963, https://doi.org/10.5194/acp-17-935-2017, 2017a.

Li, Z., Guo, J., Ding, A., Liao, H., Liu, J., Sun, Y., Wang, T., Xue, H., Zhang, H., and Zhu, B.: Aerosol and boundary-layer interactions and impact on air quality, Natl. Sci. Rev., 4, 810–833, https://doi.org/10.1093/nsr/nwx117, 2017b.

Lin, Y. L.: Bulk parameterization of the snow field in a cloud model, J. Clim. Appl. Meteorol., 22, 1065–1092, 1983.

Liu, J.: China's changing landscape during the 1990s: large-scale land transformations estimated with satellite data, Geophys. Res. Lett., 32, L02405, https://doi.org/10.1029/2004gl021649, 2005.

Liu, P. F., Zhao, C. S., Göbel, T., Hallbauer, E., Nowak, A., Ran, L., Xu, W. Y., Deng, Z. Z., Ma, N., Mildenberger, K., Henning, S., Stratmann, F., and Wiedensohler, A.: Hygroscopic properties of aerosol particles at high relative humidity and their diurnal variations in the North China Plain, Atmos. Chem. Phys., 11, 3479–3494, https://doi.org/10.5194/acp-11-3479-2011, 2011.

Liu, L. X., Huang, X., Ding, A. J., and Fu, C. B.: Dust-induced radiative feedbacks in north China: a dust storm episode modeling study using WRF-Chem, Atmos. Environ., 129, 43–54, 2016.

Mauderly, J. L. and Chow, J. C.: Health effects of organic aerosols, Inhal. Toxicol., 20, 257–288, https://doi.org/10.1080/08958370701866008, 2008.

Menon, S., Hansen, J., Nazarenko, L., and Luo, Y.: Climate effects of black carbon aerosols in China and India, Science, 297, 2250–2253, https://doi.org/10.1126/science.1075159, 2002.

Niu, F., Li, Z., Li, C., Lee, K.-H., and Wang, M.: Increase of wintertime fog in China: potential impacts of weakening of the Eastern Asian monsoon circulation and increasing aerosol loading, J. Geophys. Res., 115, D00K20, https://doi.org/10.1029/2009jd013484, 2010.

Oke, T. R.: The energetic basis of the urban heat-island, Q. J. Roy. Meteor. Soc., 108, 1–24, 1982.

Peng, J., Hu, M., Guo, S., Du, Z., Zheng, J., Shang, D., Levy Zamora, M., Zeng, L., Shao, M., Wu, Y., Zheng, J., Wang, Y., Glen, R., C., Collins, R., D., Molina, M., and Zhang, R.: Markedly enhanced absorption and direct radiative forcing of black carbon under polluted urban environments, P. Natl. Acad. Sci. USA, 113, 201602310, https://doi.org/10.1073/pnas.1602310113, 2016.

Petaja, T., Jarvi, L., Kerminen, V. M., Ding, A. J., Sun, J. N., Nie, W., Kujansuu, J., Virkkula, A., Yang, X. Q., Fu, C. B., Zilitinkevich, S., and Kulmala, M.: Enhanced air pollution via aerosol-boundary layer feedback in China, Sci. Rep.-UK, 6, 18998, https://doi.org/10.1038/srep18998, 2016.

Pope, C. A., Burnett, R. T., Thun, M. J., Calle, E. E., Krewski, D., Ito, K., and Thurston, G. D.: Lung cancer, cardiopulmonary mortality, and long-term exposure to fine particulate air pollution, Jama-J. Am. Med. Assoc., 287, 1132–1141, https://doi.org/10.1001/jama.287.9.1132, 2002.

Qin, Y. and Xie, S. D.: Estimation of county-level black carbon emissions and its spatial distribution in China in 2000, Atmos. Environ., 45, 6995–7004, https://doi.org/10.1016/j.atmosenv.2011.09.017, 2011.

Ramanathan, V. and Carmichael, G.: Global and regional climate changes due to black carbon, Nat. Geosci., 1, 221–227, https://doi.org/10.1038/ngeo156, 2008.

Shen, Y., Virkkula, A., Ding, A., Wang, J., Chi, X., Nie, W., Qi, X., Huang, X., Liu, Q., Zheng, L., Xu, Z., Petäjä, T., Aalto, P. P., Fu, C., and Kulmala, M.: Aerosol Optical Properties at SORPES in Nanjing, East China, Atmos. Chem. Phys. Discuss., https://doi.org/10.5194/acp-2017-863, in review, 2017.

Shiraiwa, M., Kondo, Y., Moteki, N., Takegawa, N., Miyazaki, Y., and Blake, D. R.: Evolution of mixing state of black carbon in polluted air from Tokyo, Geophys. Res. Lett., 34, L16803, https://doi.org/10.1029/2007gl029819, 2007.

Sun, Y., Zhuang, G., Wang, Y., Han, L., Guo, J., Dan, M., Zhang, W., Wang, Z., and Hao, Z.: The air-borne particulate pollution in Beijing – concentration, composition, distribution and sources, Atmos. Environ., 38, 5991–6004, https://doi.org/10.1016/j.atmosenv.2004.07.009, 2004.

Sun, Y. L., Jiang, Q., Wang, Z. F., Fu, P. Q., Li, J., Yang, T., and Yin, Y.: Investigation of the sources and evolution processes of severe haze pollution in Beijing in January 2013, J. Geophys. Res.-Atmos., 119, 4380–4398, https://doi.org/10.1002/2014JD021641, 2014.

Tewari, M., Chen, F., Wang, W., Dudhia, J., LeMone, M. A., Mitchell, K., Ek, M., Gayno, G., Wegiel, J., and Cuenca, R.: Implementation and verification of the united NOAH land surface model in the WRF model, 20th Conference on Weather Analysis and Forecasting/16th Conference on Numerical Weather Prediction, 2016.

Tsai, Y. I. and Kuo, S. C.: $PM_{2.5}$ aerosol water content and chemical composition in a metropolitan and a coastal area in southern Taiwan, Atmos. Environ., 39, 4827–4839, 2005.

University of Wyoming: Atmospheric Sounding database, http://weather.uwyo.edu/upperair/sounding.html,last access: 2018.

Wang, J. D., Wang, S. X., Jiang, J. K., Ding, A. J., Zheng, M., Zhao, B., Wong, D. C., Zhou, W., Zheng, G. J., Wang, L., Pleim, J. E., and Hao, J. M.: Impact of aerosol-meteorology interactions on fine particle pollution during China's severe haze episode in January 2013, Environ. Res. Lett., 9, 094002, https://doi.org/10.1088/1748-9326/9/9/094002, 2014a.

Wang, Q., Huang, R. J., Cao, J., Han, Y., Wang, G., Li, G., Wang, Y., Dai, W., Zhang, R., and Zhou, Y.: Mixing state of black carbon aerosol in a heavily polluted urban area of China: implications for light absorption enhancement, Aerosol Sci. Tech., 48, 689–697, https://doi.org/10.1080/02786826.2014.917758, 2014b.

Wang, Y. S., Yao, L., Wang, L. L., Liu, Z. R., Ji, D. S., Tang, G. Q., Zhang, J. K., Sun, Y., Hu, B., and Xin, J. Y.: Mechanism for the formation of the January 2013 heavy haze pollution episode over central and eastern China, Sci. China Earth Sci., 57, 14–25, https://doi.org/10.1007/s11430-013-4773-4, 2014c.

Wang, Z. F., Li, J., Wang, Z., Yang, W. Y., Tang, X., Ge, B. Z., Yan, P. Z., Zhu, L. L., Chen, X. S., Chen, H. S., Wand, W., Li, J. J., Liu, B., Wang, X. Y., Wand, W., Zhao, Y. L., Lu, N., and Su, D. B.: Modeling study of regional severe hazes over mid-eastern China in January 2013 and its implications on pollution prevention and control, Sci. China Earth Sci., 57, 3–13, 2014d.

Wang, J. D., Zhao, B., Wang, S. X., Yang, F. M., Xing, J., Morawska, L., Ding, A. J., Kulmala, M., Kerminen, V. M., Kujansuu, J., Wang, Z. F., Ding, D. A., Zhang, X. Y., Wang, H. B., Tian, M., Petaja, T., Jiang, J. K., and Hao, J. M.: Particulate matter pollution over China and the effects of control policies, Sci. Total Environ., 584, 426–447, 2017.

Wilcox, E. M., Thomas, R. M., Praveen, P. S., Pistone, K., Bender, F. A., and Ramanathan, V.: Black carbon solar absorption suppresses turbulence in the atmospheric boundary layer, P. Natl. Acad. Sci. USA, 113, 11794–11799, https://doi.org/10.1073/pnas.1525746113, 2016.

Xu, W. Y., Zhao, C. S., Ran, L., Deng, Z. Z., Liu, P. F., Ma, N., Lin, W. L., Xu, X. B., Yan, P., He, X., Yu, J., Liang, W. D., and Chen, L. L.: Characteristics of pollutants and their correlation to meteorological conditions at a suburban site in the North China Plain, Atmos. Chem. Phys., 11, 4353–4369, https://doi.org/10.5194/acp-11-4353-2011, 2011.

Xu, W. Y., Zhao, C. S., Ran, L., Lin, W. L., Yan, P., and Xu, X. B.: SO_2 noontime-peak phenomenon in the North China Plain, Atmos. Chem. Phys., 14, 7757–7768, https://doi.org/10.5194/acp-14-7757-2014, 2014.

Yang, L. X., Wang, D. C., Cheng, S. H., Wang, Z., Zhou, Y., Zhou, X. H., and Wang, W. X.: Influence of meteorological conditions and particulate matter on visual range impairment in Jinan, China, Sci. Total Environ., 383, 164–173, https://doi.org/10.1016/j.scitotenv.2007.04.042, 2007.

Yang, F., Chen, H., Du, J. F., Yang, X., Gao, S., Chen, J. M., and Geng, F. H.: Evolution of the mixing state of fine aerosols during haze events in Shanghai, Atmos. Res., 104, 193–201, https://doi.org/10.1016/j.atmosres.2011.10.005, 2012.

Yang, Y., Liu, X., Qu, Y., Wang, J., An, J., Zhang, Y., and Zhang, F.: Formation mechanism of continuous extreme haze episodes in the megacity Beijing, China, in January 2013, Atmos. Res., 155, 192–203, https://doi.org/10.1016/j.atmosres.2014.11.023, 2015.

Yang, X., Zhao, C. F., Zhou, L. J., Wang, Y., and Liu, X. H.: Distinct impact of different types of aerosols on surface solar radiation in China, J. Geophys. Res.-Atmos., 121, 6459–6471, 2016.

Ye, B., Ji, X., Yang, H., Yao, X., Chan, C. K., Cadle, S. H., Chan, T., and Mulawa, P. A.: Concentration and chemical composition of $PM_{2.5}$ in Shanghai for a 1 year period, Atmos. Environ., 37, 499–510, https://doi.org/10.1016/S1352-2310(02)00918-4, 2003.

Yu, H. B., Liu, S. C., and Dickinson, R. E.: Radiative effects of aerosols on the evolution of the atmospheric boundary layer, J. Geophys. Res.-Atmos., 107, 4142, https://doi.org/10.1029/2001jd000754, 2002.

Zaveri, R. and Peters, L., K.: Anew lumped structure photochemical mechanism for long-scale applications, J. Geophys. Res.-Atmos., 104, 30387–30415, https://doi.org/10.1029/1999JD900876, 1999.

Zaveri, R. A., Easter, R. C., Fast, J. D., and Peters, L. K.: Model for Simulating Aerosol Interactions and Chemistry (MOSAIC), J. Geophys. Res.-Atmos., 113, D13204, https://doi.org/10.1029/2007jd008782, 2008.

Zhang, Q., Ma, X., Tie, X., Huang, M., and Zhao, C.: Vertical distributions of aerosols under different weather conditions: analysis of in-situ aircraft measurements in Beijing, China, Atmos. Environ., 43, 5526–5535, https://doi.org/10.1016/j.atmosenv.2009.05.037, 2009a.

Zhang, Q., Streets, D. G., Carmichael, G. R., He, K. B., Huo, H., Kannari, A., Klimont, Z., Park, I. S., Reddy, S., Fu, J. S., Chen, D., Duan, L., Lei, Y., Wang, L. T., and Yao, Z. L.: Asian emissions in 2006 for the NASA INTEX-B mission, Atmos. Chem. Phys., 9, 5131–5153, https://doi.org/10.5194/acp-9-5131-2009, 2009b.

Zhang, X. Y., Wang, Y. Q., Niu, T., Zhang, X. C., Gong, S. L., Zhang, Y. M., and Sun, J. Y.: Corrigendum to "Atmospheric aerosol compositions in China: spatial/temporal variability, chemical signature, regional haze distribution and comparisons with global aerosols" published in Atmos. Chem. Phys., 12, 779–799, 2012, Atmos. Chem. Phys., 12, 6273–6273, https://doi.org/10.5194/acp-12-6273-2012, 2012.

Zhang, R., Jing, J., Tao, J., Hsu, S.-C., Wang, G., Cao, J., Lee, C. S. L., Zhu, L., Chen, Z., Zhao, Y., and Shen, Z.: Chemical characterization and source apportionment of $PM_{2.5}$ in Beijing: seasonal perspective, Atmos. Chem. Phys., 13, 7053–7074, https://doi.org/10.5194/acp-13-7053-2013, 2013.

Zhang, H., Wang, S., Hao, J., Wang, X., Wang, S., Chai, F., and Li, M.: Air pollution and control action in Beijing, J. Clean. Prod., 112, 1519–1527, https://doi.org/10.1016/j.jclepro.2015.04.092, 2016.

Zhao, P. S., Zhang, X. L., and Xu, X. F.: Long-term visibility trends and characteristics in the region of Beijing, Tianjin, and Hebei, China, Abstr. Pap. Am. Chem. S., 242, 711–718, https://doi.org/10.1016/j.atmosres.2011.04.019, 2011.

Zhao, P. S., Dong, F., He, D., Zhao, X. J., Zhang, X. L., Zhang, W. Z., Yao, Q., and Liu, H. Y.: Characteristics of concentrations and chemical compositions for $PM_{2.5}$ in the region of Beijing, Tianjin, and Hebei, China, Atmos. Chem. Phys., 13, 4631–4644, https://doi.org/10.5194/acp-13-4631-2013, 2013a.

Zhao, X. J., Zhao, P. S., Xu, J., Meng,, W., Pu, W. W., Dong, F., He, D., and Shi, Q. F.: Analysis of a winter regional haze event and its formation mechanism in the North China Plain, Atmos. Chem. Phys., 13, 5685–5696, https://doi.org/10.5194/acp-13-5685-2013, 2013b.

Zhao, D. L., Tie, X. X., Gao, Y., Zhang, Q., Tian, H. J., Bi, K., Jin, Y. L., and Chen, P. F.: In-situ aircraft measurements of the vertical distribution of black carbon in the lower troposphere of Beijing, China, in the spring and summer time, Atmosphere-Basel, 6, 713–731, https://doi.org/10.3390/atmos6050713, 2015.

Zheng, G. J., Duan, F. K., Su, H., Ma, Y. L., Cheng, Y., Zheng, B., Zhang, Q., Huang, T., Kimoto, T., Chang, D., Pöschl, U., Cheng, Y. F., and He, K. B.: Exploring the severe winter haze in Beijing: the impact of synoptic weather, regional transport and heterogeneous reactions, Atmos. Chem. Phys., 15, 2969–2983, https://doi.org/10.5194/acp-15-2969-2015, 2015.

Zhi, G. R., Chen, Y. J., Feng, Y. L., Xiong, S. C., Li, J., Zhang, G., Sheng, G. Y., and Fu, J.: Emission characteristics of carbonaceous particles from various residential coal-stoves in China, Environ. Sci. Technol., 42, 3310–3315, 2008.